

Article

Effect of Rotational Speed on Tribological Properties of Carbon Fiber-Reinforced Al-Si Alloy Matrix Composites

Feng Tang , Xiaotao Pan ^{*}, Yafei Deng, Zhenquan Zhou, Guoxun Zeng and Sinong Xiao

School of Materials and Energy, Guangdong University of Technology, Guangzhou 510006, China

^{*} Correspondence: xtpan@gdut.edu.cn

Abstract: Porous carbon fiber-reinforced Al-Si alloy matrix composites and carbon fiber felt-reinforced Al-Si alloy matrix composites with carbon content of 10 wt.% were prepared by die casting. The dry tribological properties of these two composites and Al-Si alloy were studied using a ball-on-disc rotational tribometer in the rotational speed range of 300 r/min to 1000 r/min, and the wear mechanisms were analyzed in combination with the wear morphology. The results show that the friction coefficient and wear rate of these two composites are lower than the Al-Si alloy at different speeds. With the increase in rotational speed, the friction coefficient of the two composites and Al-Si alloy first increases and then decreases, and the wear rate gradually increases. The wear mechanisms of the two composites and Al-Si alloy change from abrasive wear and adhesive wear to delamination wear, but the node speed of the change in the wear mechanism of the composites to delamination wear is higher, and the wear degree is relatively slight. In addition, the comprehensive tribological properties of carbon fiber felt-reinforced Al-Si alloy matrix composites are better than the porous carbon fiber-reinforced Al-Si alloy matrix composites.

Keywords: die casting; carbon fiber; Al-Si alloy matrix composite; rotational speed; tribological property



Citation: Tang, F.; Pan, X.; Deng, Y.; Zhou, Z.; Zeng, G.; Xiao, S. Effect of Rotational Speed on Tribological Properties of Carbon Fiber-Reinforced Al-Si Alloy Matrix Composites. *Lubricants* **2023**, *11*, 142. <https://doi.org/10.3390/lubricants11030142>

Received: 22 February 2023

Revised: 9 March 2023

Accepted: 15 March 2023

Published: 17 March 2023



Copyright: © 2023 by the authors. Licensee MDPI, Basel, Switzerland. This article is an open access article distributed under the terms and conditions of the Creative Commons Attribution (CC BY) license (<https://creativecommons.org/licenses/by/4.0/>).

1. Introduction

Al-Si alloy is widely used in automobile, aviation, aerospace, and other industries due to its advantages of low density, high specific strength, low thermal expansion coefficient, good casting performance, good weldability, and easy forming [1–3]. Nevertheless, the use of Al alloy for a wider range of applications is limited due to its deficiency in terms of tribological properties [4–6]. Carbon fiber (CF) is a reinforcement with excellent mechanical properties, thermal conductivity, and self-lubricating ability [7–9]. Asano et al. [10] studied the wear behavior of CF-reinforced Al alloy matrix (Al/CF) composites under dry sliding conditions, and the results showed that the coefficient of friction (COF) and wear loss of the alloy are decreased due to the fiber reinforcement and the crumbled CFs forming a solid lubricant film on the worn surfaces. Sree Manu et al. [11] concluded that the wear rate of Al/CF composite is significantly lower compared to Al alloy due to the incorporation of CF, which suppresses the transition to a severe wear rate. By making Al-Si alloy and CF into a composite, the advantages of Al-Si alloy and CF can complement each other, which can break through the limitations of the application of Al alloy in the field of tribology. Recently, much work has been focused on investigating the effect of CF on the mechanical and thermal properties of Al-Si alloys [12–14]. However, the tribological properties of Al-Si/CF composites have been rarely studied.

Compared with the solid state method [15–17], the liquid state method used to prepare CF-reinforced Al matrix composites has the outstanding advantages of high production efficiency, low cost, and suitability for large-scale production [18–20]. However, due to the poor wettability between CF and Al matrix, it is difficult for the Al melt to penetrate the inner region of the CF bundle by the liquid method [21]. From the manufacturing

perspective, increasing the process temperature and working pressure are two effective solutions for the above problem [22,23]. However, increasing the process temperature will intensify the harmful interfacial reaction between the CF and the Al matrix, which can generate a lot of Al_4C_3 . The generated Al_4C_3 will seriously damage the interfacial structure, resulting in reduced mechanical properties of composites [24–26]. Therefore, increasing the working pressure has been the ultimate solution to the problem of poor wettability. Compared with other casting processes, the pressure die casting process is the ideal choice for the preparation of Al-Si/CF composites because it can provide considerable working pressure and manufacture components of high complexity and high precision, and can be cooled quickly to refine grains [20,27]. It also has competitive cost and production efficiency advantages. Nevertheless, despite the advantages of die casting, few studies have used this process to manufacture Al matrix composites. Recently, Bedmar et al. [27] prepared CF fabric-reinforced Al matrix composites by using a die casting process for the first time. The high pressure applied by the die casting process allowed full wetting of the CFs, and the composites were practically free from defects.

The tribological properties of Al/CF composites are mainly affected by factors such as carbon fiber content, applied load, temperature, and rotational speed. Eid et al. [28] reported the effect of different carbon fiber contents on the tribological properties of Al/CF composites, and the results indicated that the wear rate and COF of the composites are lowest when the carbon fiber content is 10 wt.%. In our previous study, it was confirmed that the carbon felt-reinforced Al-Si alloy composites still exhibited excellent wear properties in the temperature range of 25–350 °C, and the wear mechanism of the composite changed from abrasive wear to oxidative wear with the increase in temperature [29]. Liu et al. and Du et al. [30,31] found that with the increase in load or temperature, the wear mechanism of Al_2O_3 and carbon short fiber-reinforced Al-12Si alloy hybrid composites changed from furrow wear to severe adhesive wear, and the wear loss continued to increase. Al-Si/CF self-lubricating composites are mainly considered to be used in the manufacture of moving parts, such as pistons, bearing bushes, brake rotors, brake discs, and bearings [32,33]. The effect of rotational speed on the tribological properties of these rotating parts cannot be ignored. Studying the effect of rotational speed on the tribological properties of Al-Si/CF composites, which is of great significance in predicting and improving the lifetime of rotating parts made of such composites, but it has been rarely reported specifically. Based on the above considerations, Al-Si/CF composites were prepared by the die casting process, and the effect of rotational speed on the tribological properties of Al-Si/CF composites was closely studied.

2. Experimental Materials and Methods

2.1. Preparation of Composite Materials

The Al-Si/CF composites were prepared by a J-1114 horizontal cold chamber die casting machine using the Al-Si alloy (Al-Si5Cu1Mg) as the matrix and the CF as the reinforcement. To enhance the infiltration effect, two kinds of CF with a diameter of 20 μm were selected. One was porous carbon fiber (CF_p) prepared by chemical activation method, and the other was carbon fiber felt (CF_f) woven from CF filaments, which are made into prefabricated parts with a diameter of 40 mm. The microstructures of CF_p and CF_f are shown in Figure 1. Firstly, the Al-Si alloy ingot was heated to 690 °C to melt, and then the molten Al-Si alloy metal liquid was pressed into the cavity of the die-casting mold with the CF prefabricated part at an injection pressure of 65 MPa, and the sample was removed after maintaining pressure for 30 s. An Al-Si/ CF_p composite and Al-Si/ CF_f composite with a carbon content of 10 wt.% were obtained. The Al-Si alloy samples were prepared using the same method.

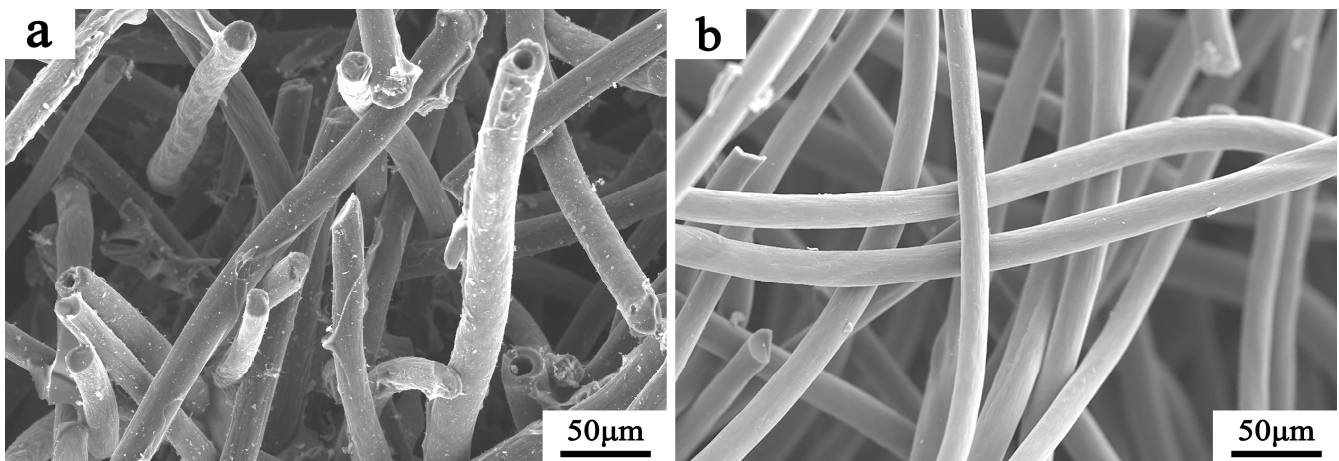


Figure 1. Microstructures of two CFs: (a) CF_p; (b) CF_f.

2.2. Microstructure Characterization and Physical Properties Test

The phase compositions of the composites and the Al-Si matrix alloys were identified by an X-ray diffractometer (XRD, D/MAX-Ultima IV, Rigaku, Tokyo, Japan) with Cu K α radiation source at a speed of 8°/min from 10° to 90°. The microstructure and chemical compositions were analyzed by scanning electron microscope (SEM, S-3400N-II, Hitachi, Tokyo, Japan) equipped with Energy Dispersive Spectrometer (EDS). The microhardness was assessed using a Vickers hardness tester (HVS 1000Z, Haoxinda Instrument, Shenzhen, China) under a load of 3 N for 15 s, and evaluated via an average value from 10 measured points at different regions of the sample. The density of the samples was determined by the Archimedes drainage method. The thermal conductivity of the sample from room temperature to 300 °C was measured by an interface material thermal resistance thermal conductivity tester (DXF-200, Waters, Milford, MA, USA). The density and the thermal conductivity of the samples were calculated by an average value from 5 measured samples.

2.3. Wear Test

A dry-sliding wear test was conducted on a ball-on-disc rotational tribometer (HT-1000, Zhongke Kaihua Technology Development, Lanzhou, China). A GCr15 ball with a diameter of 6 mm was chosen as the counterpart ball due to its high hardness and good wear resistance (56 HRC). A schematic diagram of the ball-on-disc rotational tribometer is shown in Figure 2. The applied load was 8 N, the rotating radius was 4 mm, and the wear test was continued for 30 min at room temperature at rotational speeds of 300, 500, 800, and 1000 r/min. The COF curves with sliding time were recorded by using a computer program. The wear rate was calculated by measuring the mass of the sample before and after the wear test. The worn surfaces and chemical composition were analyzed by SEM and EDS.

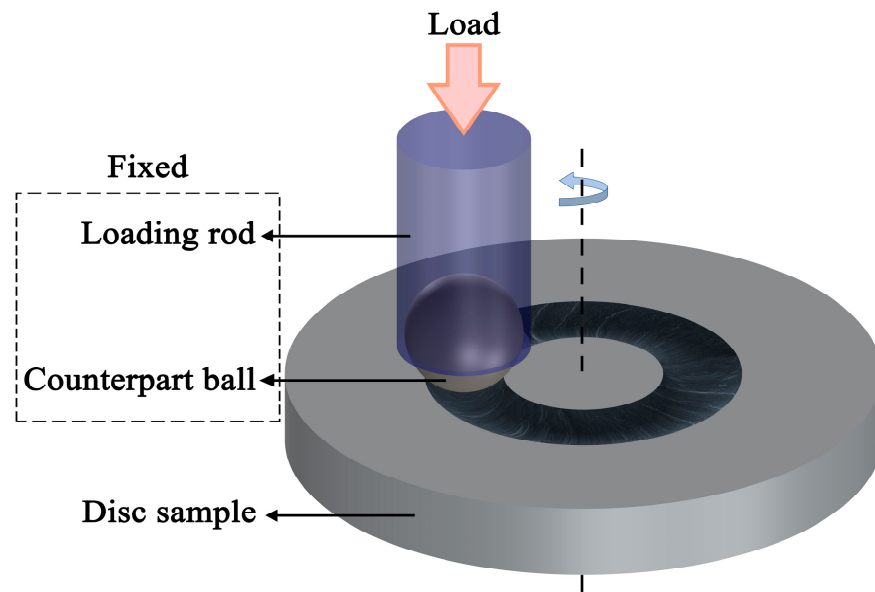


Figure 2. Schematic diagram of ball-on-disc rotational tribometer.

3. Results and Discussion

3.1. Microstructure Characteristics

Figure 3 shows the XRD patterns of Al-Si alloy and Al-Si/CF_p, Al-Si/CF_f composites. The results show that the diffraction peaks of α -Al and single-crystal Si are detected in the Al-Si alloy. With the addition of CFs, the diffraction peaks of C appear in both composites, but no evidence of the brittle phase Al₄C₃ exists in any of the composites. The die casting process can provide high working pressure to accelerate the wetting rate of Al liquid and CF, shorten the contact time of Al-Si alloy and CF at high temperatures, and minimize the interface reaction, thus reducing the formation of Al₄C₃ phase. Moreover, the presence of a small amount of Si, Cu, Mg elements in the matrix can also inhibit the formation of Al₄C₃, so the Al₄C₃ diffraction peak is not detected in both composites [34–38].

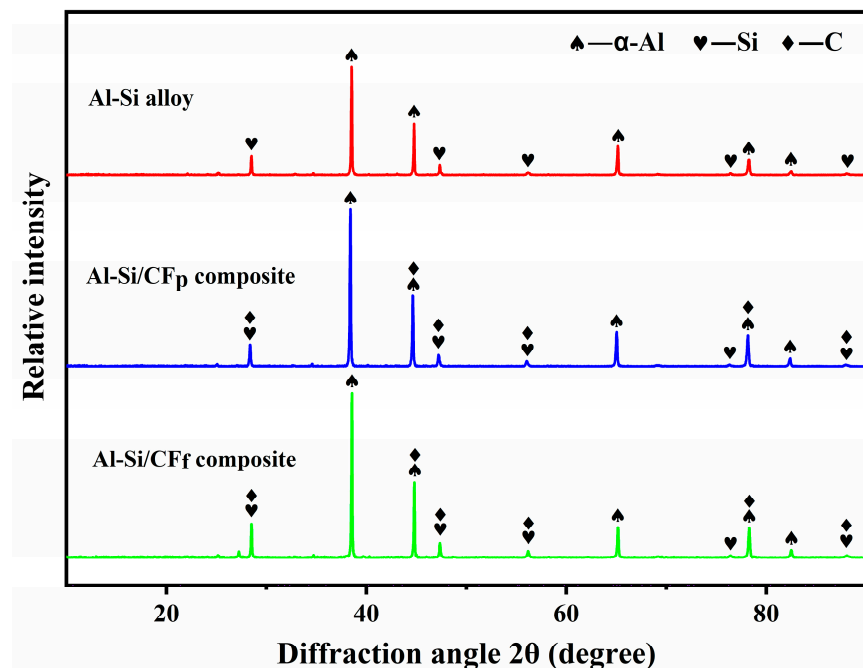


Figure 3. XRD patterns of Al-Si alloy and Al-Si/CF_p, Al-Si/CF_f composites.

The SEM images and EDS maps of the Al-Si/CF_f, Al-Si/CF_p composites and Al-Si alloys are shown in Figure 4. The solid lubricant CF and hard phase Si are uniformly dispersed in the Al-Si alloy matrix, forming a good wear-reducing and wear-resistant structure.

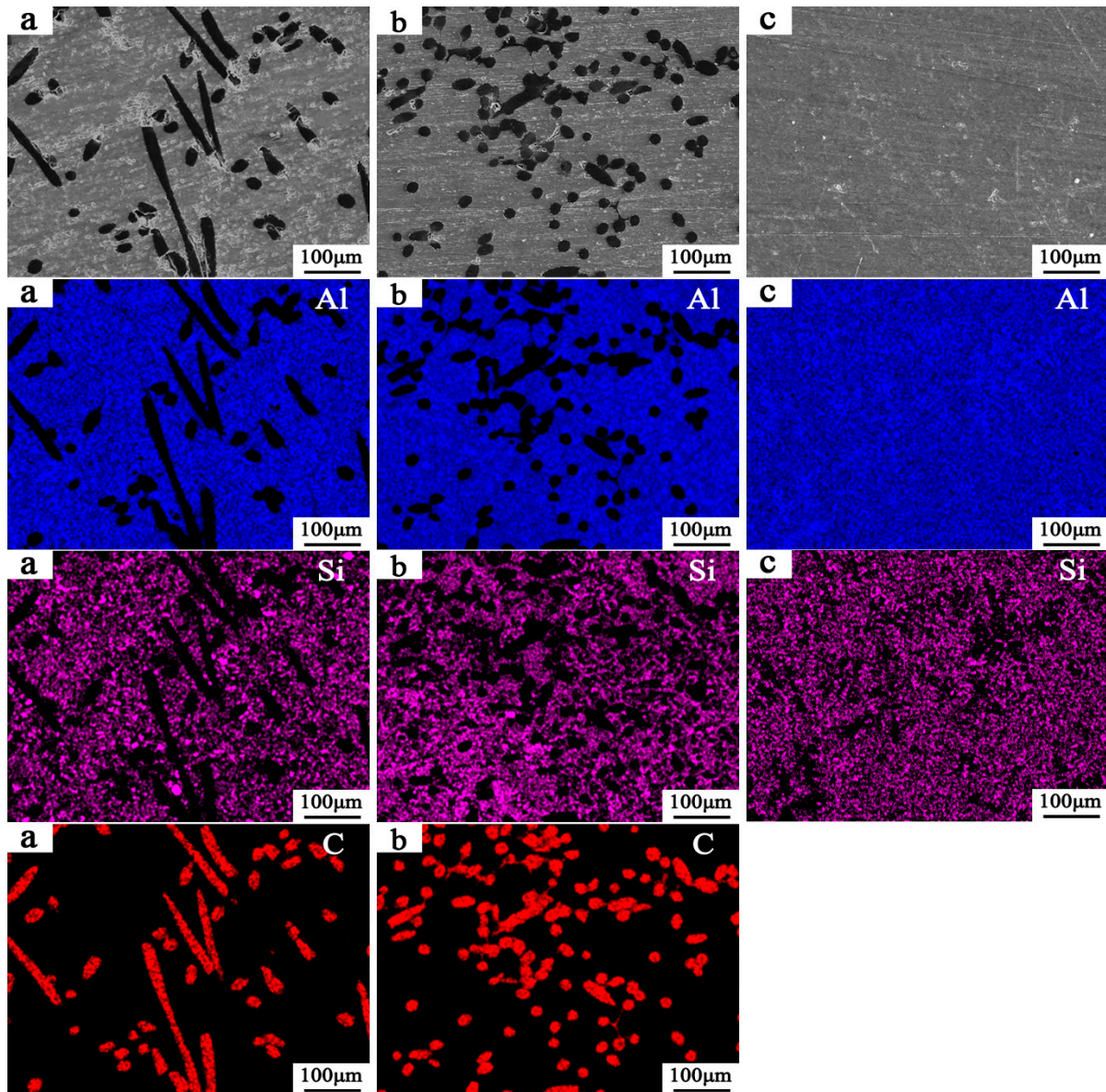


Figure 4. SEM images and EDS maps of samples: (a) Al-Si/CF_f composite; (b) Al-Si/CF_p composites; (c) Al-Si alloy.

3.2. Physical Properties

The density, Vickers hardness, and thermal conductivity of Al-Si alloy and Al-Si/CF_p, Al-Si/CF_f composites are presented in Table 1. Compared with the Al-Si alloy, the density of the two composites decreases while the hardness increases slightly, which can be attributed to the low density of CF compared to Al-Si alloy [39], and the CFs restrict the grain growth and restrain the plastic flow behavior of the matrix [11,27,28]. Furthermore, the thermal conductivity of the two composites is significantly higher than that of the Al-Si alloy, which is attributed to the excellent thermal conductivity of CFs in the composites [40,41]. The hardness and thermal conductivity of the two composites are similar. However, the density of the Al-Si/CF_p composite is only 92% of that of the Al-Si/CF_f composite, which is because

the apparent density of the CF_p is lower than that of the CF_f due to its hollow porous structure [42].

Table 1. Physical properties of Al-Si alloy and Al-Si/CF_p, Al-Si/CF_f composites.

Material	Density (g/cm ³)	Vickers Hardness (HV)	Thermal Conductivity (W/(m·K))
Al-Si alloy	2.62	85.04	142.92 ± 1.85
Al-Si/CF _p composite	2.32	86.39	178.11 ± 5.53
Al-Si/CF _f composite	2.51	87.28	178.85 ± 2.45

3.3. Tribological Properties

3.3.1. COF

Figure 5 shows the COF curves of the Al-Si alloy and Al-Si/CF_p, Al-Si/CF_f composites at various rotational speeds. In the initial stage of friction, the COF rises sharply and then decreases rapidly, and the amplitude of the fluctuation of the COF is large in the following short period of time, and then the COF curve gradually flattens out. This stage is the running-in period of the material; a similar phenomenon has been reported by other researchers [43,44]. Compared with the Al-Si alloy, the Al-Si/CF_p and Al-Si/CF_f composites have a shorter running-in period and more gentle COF curves in the stable friction stage, which indicates that the addition of CFs plays an important role in stabilizing the COF [45]. On the one hand, the CF can produce carbon film with a certain lubricating effect; on the other hand, the CF with excellent thermal conductivity can dissipate the heat generated by friction from around the friction pair in time, reducing the softening effect of the composite material due to temperature rise [46,47]. This explains why the COF of the Al-Si alloy fluctuates greatly in the later stage of the friction experiment.

The variation law of the average COF of Al-Si alloy and Al-Si/CF_p, Al-Si/CF_f composites with rotational speed are shown in Figure 6. It can be observed that the COF of Al-Si/CF_f and Al-Si/CF_p composites is significantly lower than that of Al-Si alloys, which benefits from the excellent lubricity of the CFs. The COF of the Al-Si/CF_f composite is lower than that of the Al-Si/CF_p composite, indicating that the CF_f has a better lubricating effect than the CF_p. Furthermore, the average COF of the Al-Si alloy and Al-Si/CF_p, Al-Si/CF_f composites shows a trend of first increasing and then decreasing with the increase in rotational speed. Among them, the COF of Al-Si alloy and Al-Si/CF_p composite have the maximum value at 500 r/min with 0.507 and 0.323, respectively, while the COF of Al-Si/CF_f composite reaches the maximum value of 0.225 at 800 r/min. Under the same load, the effect of rotational speed on the COF of Al-Si/CF composites mainly depends on the formation of carbon film and the change in the surface temperature of the friction pair. At low rotational speed, the COF is lower because it forms a relatively complete carbon film. With the increase in rotational speed, the contact surface of the friction pair appears to exhibit local adhesion, and the carbon film is destroyed, resulting in an increase in the COF. At high rotational speed, a large amount of heat will accumulate on the contact surface of the friction pair, causing the surface material of the friction pair to soften, thereby reducing the COF.

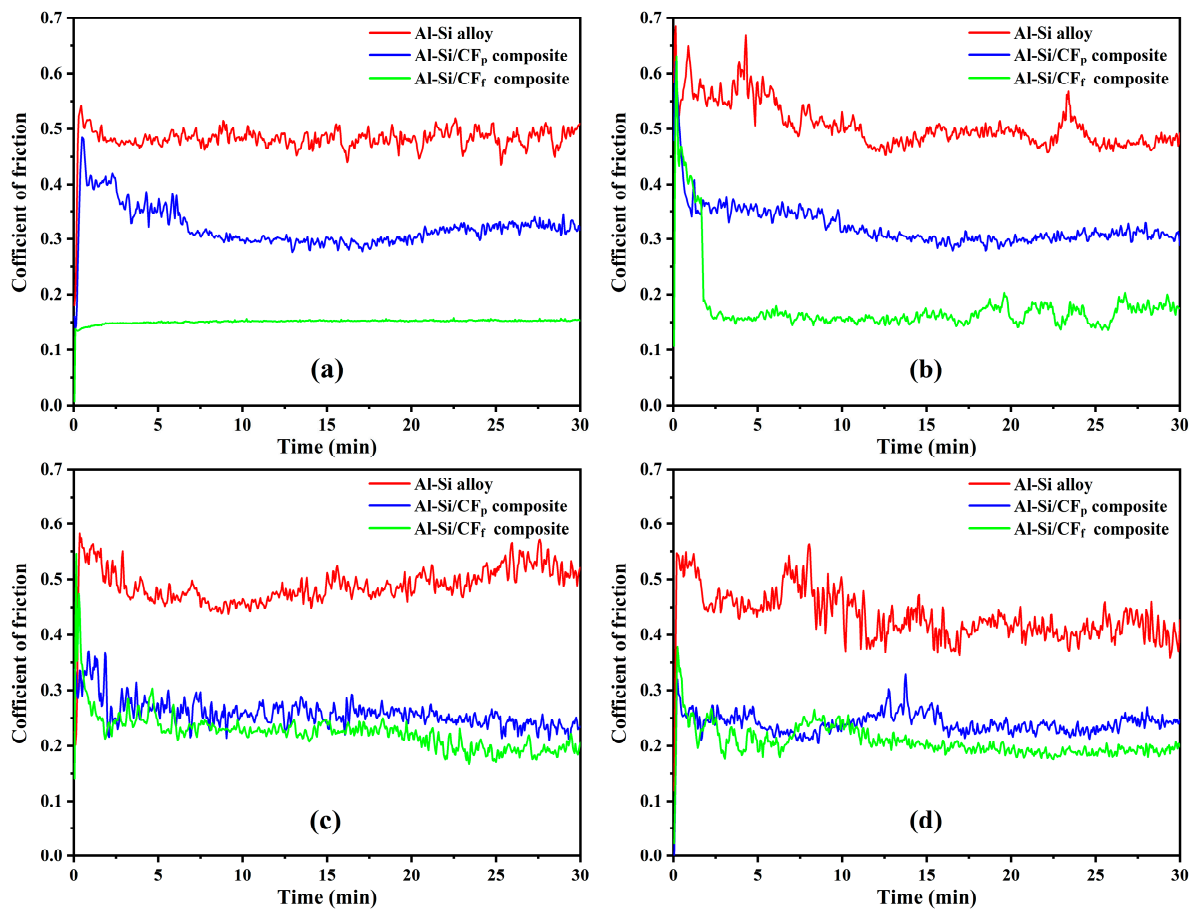


Figure 5. COF curves of Al-Si alloy and Al-Si/CF_r, Al-Si/CF_p composites at various rotational speeds: (a) 300 r/min; (b) 500 r/min; (c) 800 r/min; (d) 1000 r/min.

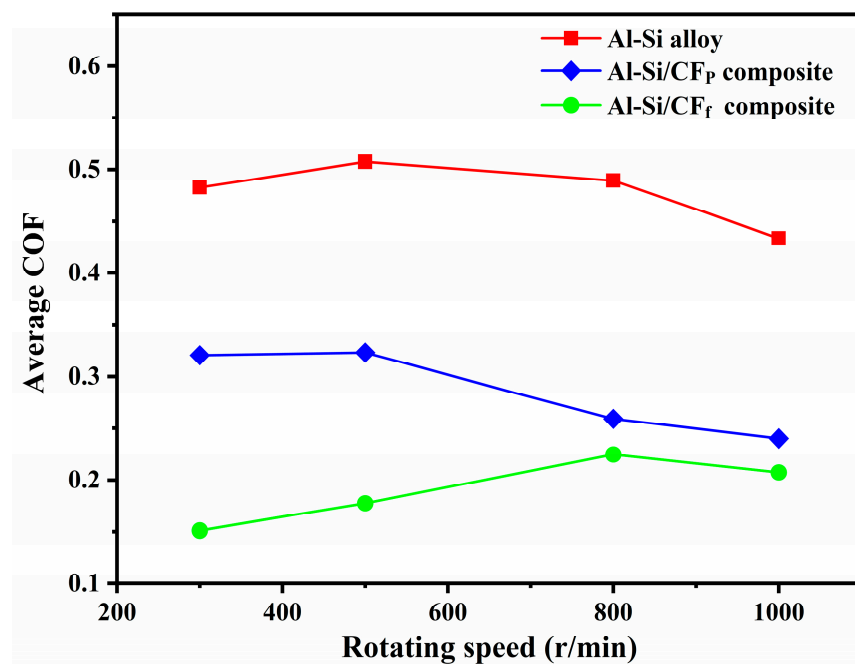


Figure 6. Average COF of Al-Si alloy and Al-Si/CF_p, Al-Si/CF_r composites at various rotational speeds.

3.3.2. Wear Rate

The wear rates of Al-Si alloy and Al-Si/CF_p, Al-Si/CF_f composites at various rotational speeds are shown in Figure 7. It is obvious that the wear rates of all three materials increase with the increase in rotational speed, which is consistent with the findings of other researchers [11,46]. Furthermore, the wear rate of the Al-Si alloy has a faster growth rate compared to the composites. The wear rate of the Al-Si alloy is $3.206 \times 10^{-3} \text{ mm}^3\text{m}^{-1}$ at 300 r/min, and the wear rate doubles to $6.631 \times 10^{-3} \text{ mm}^3\text{m}^{-1}$ at 1000 r/min. Furthermore, the wear rate of both composites is lower than that of the Al-Si alloy at different rotational speeds, and the wear rate of the Al-Si/CF_f composite is slightly lower than that of the Al-Si/CF_p composite. This indicates that the CFs play an important role in mitigating the effect of rotational speed on the wear of Al-Si/CF composites and in reducing the wear rate of Al-Si/CF composites.

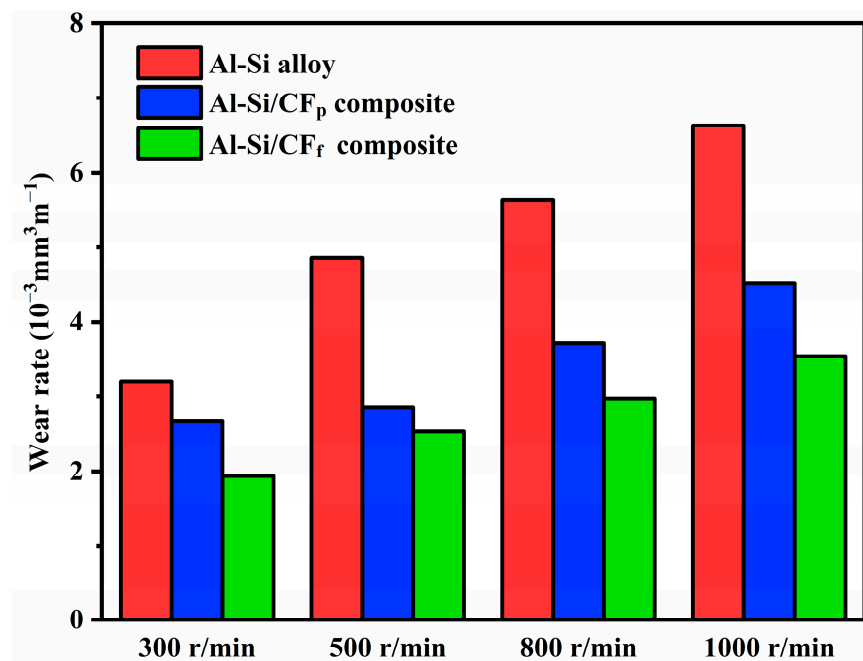


Figure 7. Wear rate of Al-Si alloy and Al-Si/CF_p, Al-Si/CF_f composites at various rotational speeds.

3.3.3. Worn Surface Morphology

Figure 8 shows the SEM images of the worn surface morphologies of Al-Si alloy at various rotational speeds. At a rotational speed of 300 r/min, the Al-Si alloy is in the stage of slight wear, and the worn surface is relatively smooth, with some shallow scratches and a few small adhesion pits, indicating that the wear mechanisms are mainly abrasive wear and slight adhesive wear (Figure 8a). Since the Al-Si alloy is exposed to the air, its surface will make full contact with the air, and a brittle and hard alumina protective film will quickly be formed. The surface of the Al-Si alloy is quite smooth and the COF and wear rate of Al-Si alloy are reduced, which is attributed to the existence of oxide film in this layer. When the rotational speed is increased to 500 r/min, the worn surface of the Al-Si alloy is rough and severely torn, and large adhesion pits are formed (Figure 8b). As shown in Figure 9, the SEM images and EDS maps of the worn surface of the counterpart ball against the Al-Si alloy at 500 r/min also show that there are many stickies on the counterpart ball, and the EDS mappings can confirm that the stickers are Al-Si alloy. The above evidence indicates that serious adhesion wear occurred, and the COF and wear rate increase due to the oxide layer caused by adhesive wear being destroyed.

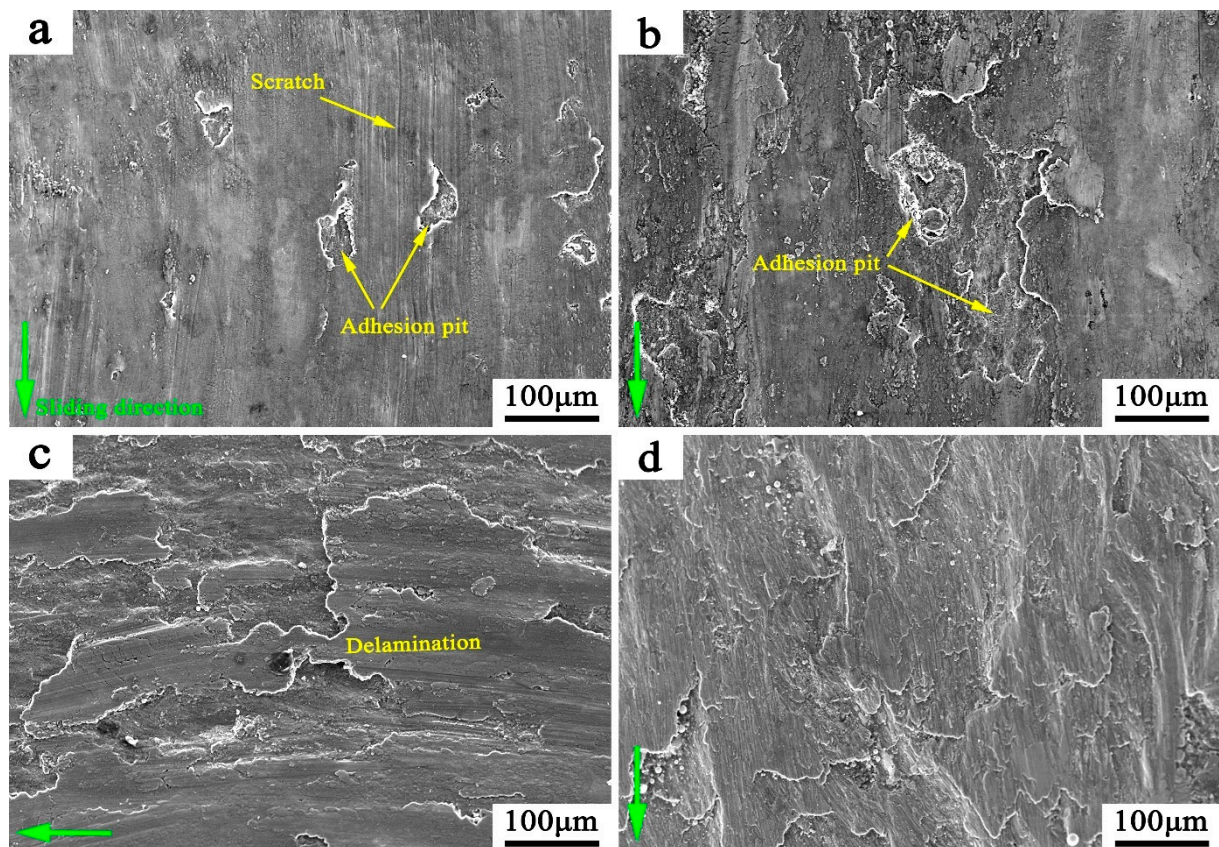


Figure 8. SEM images of the worn surface morphologies of Al-Si alloy at various rotational speeds: (a) 300 r/min; (b) 500 r/min; (c) 800 r/min; (d) 1000 r/min.

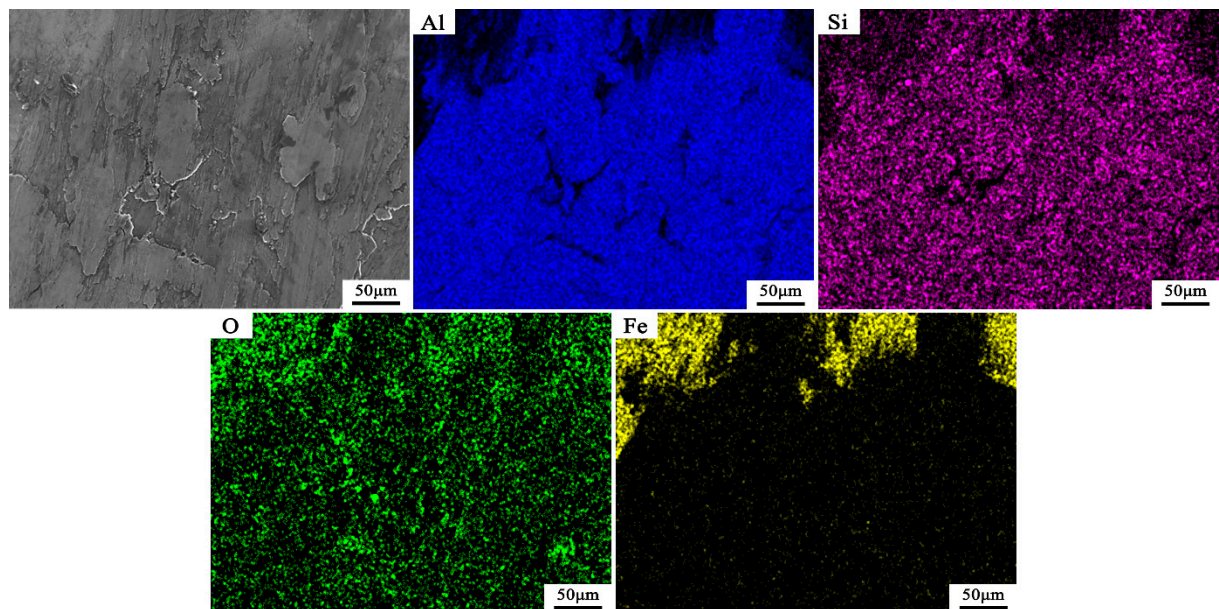


Figure 9. SEM images and EDS maps of worn surface of the counterpart ball against the Al-Si alloy at 500 r/min.

At the rotational speeds of 800 r/min and 1000 r/min, the worn surface of the Al-Si alloy appeared irregular due to the delamination and exfoliation of large pieces of material, indicating that the delamination wear caused by severe plastic deformation is the main

wear mechanism (Figure 8c,d). At relatively high rotational speed, the temperature on the surface of the friction pair increases sharply because the heat generated by friction is difficult to transmit in time, which causes heat accumulation on the surface of the friction pair. As a result, the surface layer material of Al-Si alloy softens, which promotes the substantial expansion of microcracks in the subsurface layer, resulting in serious lamellar peeling of the material of the friction surface layer, which is characterized by peeling wear and a high wear rate.

Figure 10 shows the SEM images of the worn surface morphologies of Al-Si/CF_p composites at various rotational speeds. At the rotational speeds of 300 r/min and 500 r/min, there are many shallow scratches and adhesion pits on the worn surface of the Al-Si/CF_p composite (Figure 10a,b). As shown in Figure 11, the SEM images and EDS maps of the worn surface of the counterpart ball against the Al-Si/CF_p composite at 500 r/min. The Al-Si/CF_p composite largely adheres to the surface of the counterpart ball and the carbon particles can be observed, indicating that the wear mechanisms are mainly abrasive wear and adhesion wear. On the worn surface, the CFs protrude continuously because the softer matrix is worn in advance. Under the action of the counterpart ball and wear debris, the protruding CFs are broken into tiny carbon particles. These lubricating carbon particles are diffused between the composite and the counterpart ball, and form a solid lubricating film on the surface of the friction pair. This lubricating film avoids rubbing directly by metal-metal and effectively reducing the loss of the composite in the process of wear.

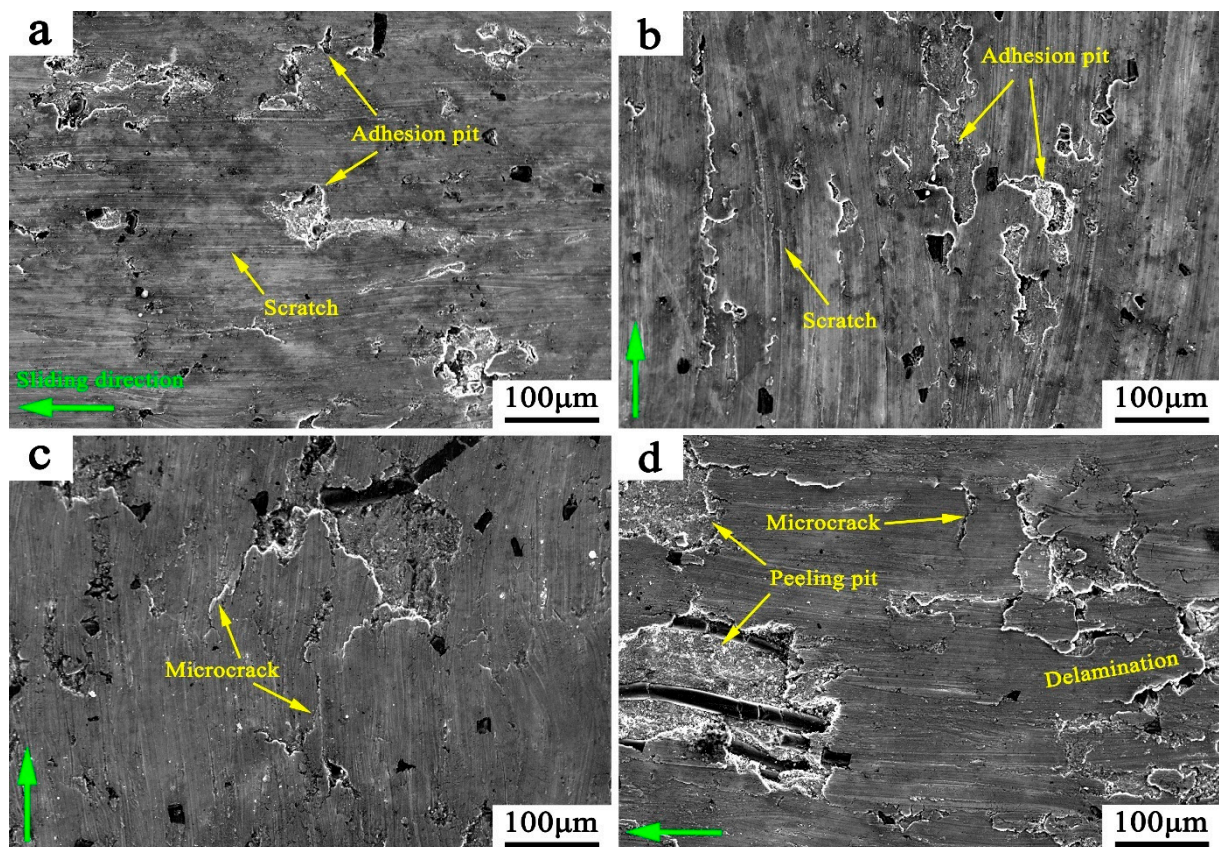


Figure 10. SEM images of the worn surface morphologies of Al-Si/CF_p composites at various rotational speeds: (a) 300 r/min; (b) 500 r/min; (c) 800 r/min; (d) 1000 r/min.

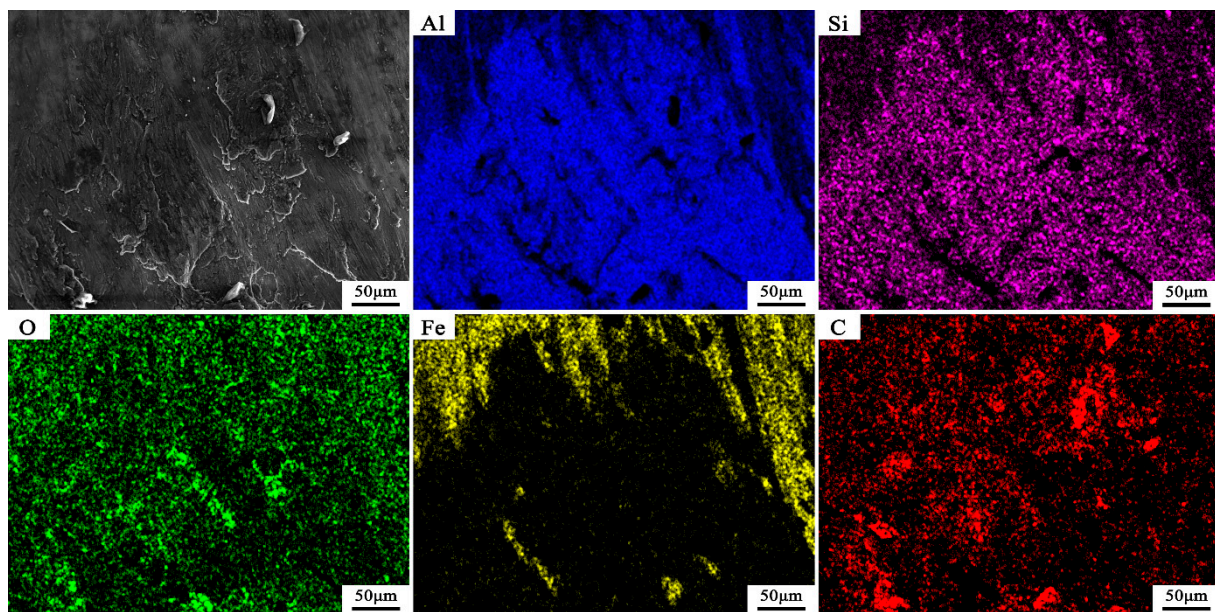


Figure 11. SEM images and EDS maps of worn surface of the counterpart ball against the Al-Si/CF_p composite at 500 r/min.

The worn surface of Al-Si/CF_p composites has shallow grooves, microcracks, and deep peeling pits at the rotational speed of 800 r/min (Figure 10c), which tends to change to delamination wear, but it is still mainly abrasive wear and adhesive wear. However, at the rotational speed of 1000 r/min, deep flaky peeling pits appear on the worn surface of the Al-Si/CF_p composite, and the CFs are also exposed. In addition, the worn surface also shows wide cracks and the material of the surface layer is loosened, indicating that the wear mechanism has changed to delamination wear (Figure 10d).

Figure 12 shows the SEM images of the worn surface morphologies of Al-Si/CF_f composites at various rotational speeds. At a rotational speed of 300 r/min, the worn surface of the Al-Si/CF_f composite has many shallow grooves caused by the counterpart balls and wear debris, which is a typical abrasive wear characteristic (Figure 12a). At 500 r/min, in addition to many shallow grooves, a small amount of adhesion pits appeared on the worn surface of the Al-Si/CF_f composite (Figure 12b). Figure 13 shows the SEM images and EDS maps of the worn surface of the counterpart ball against the Al-Si/CF_p composite at 500 r/min. Similar to the Al-Si/CF_p composite, CF_f exerts an excellent lubricating effect and forms a solid lubricating film. However, unlike the Al-Si/CF_p composite, the Al-Si/CF_f composite had less adhesion on the surface of the counterpart ball, indicating that slight adhesive wear occurs in the Al-Si/CF_f composite. When the rotational speed reaches 800 r/min, the degree of adhesive wear of the Al-Si/CF_f composite is obviously intensified (Figure 12c). At 1000 r/min, the worn surface of the Al-Si/CF_f composite is relatively smooth, and some flaky surface layers tend to be peeled off. Furthermore, the adhesion pits and the peeling pits coexist on the worn surface of the Al-Si/CF_f composite, and CFs can be found at the edges of the peeling pits (Figure 12d), which indicates that the wear mechanism of the Al-Si/CF_f composite is changing from adhesive wear to slight delamination wear.

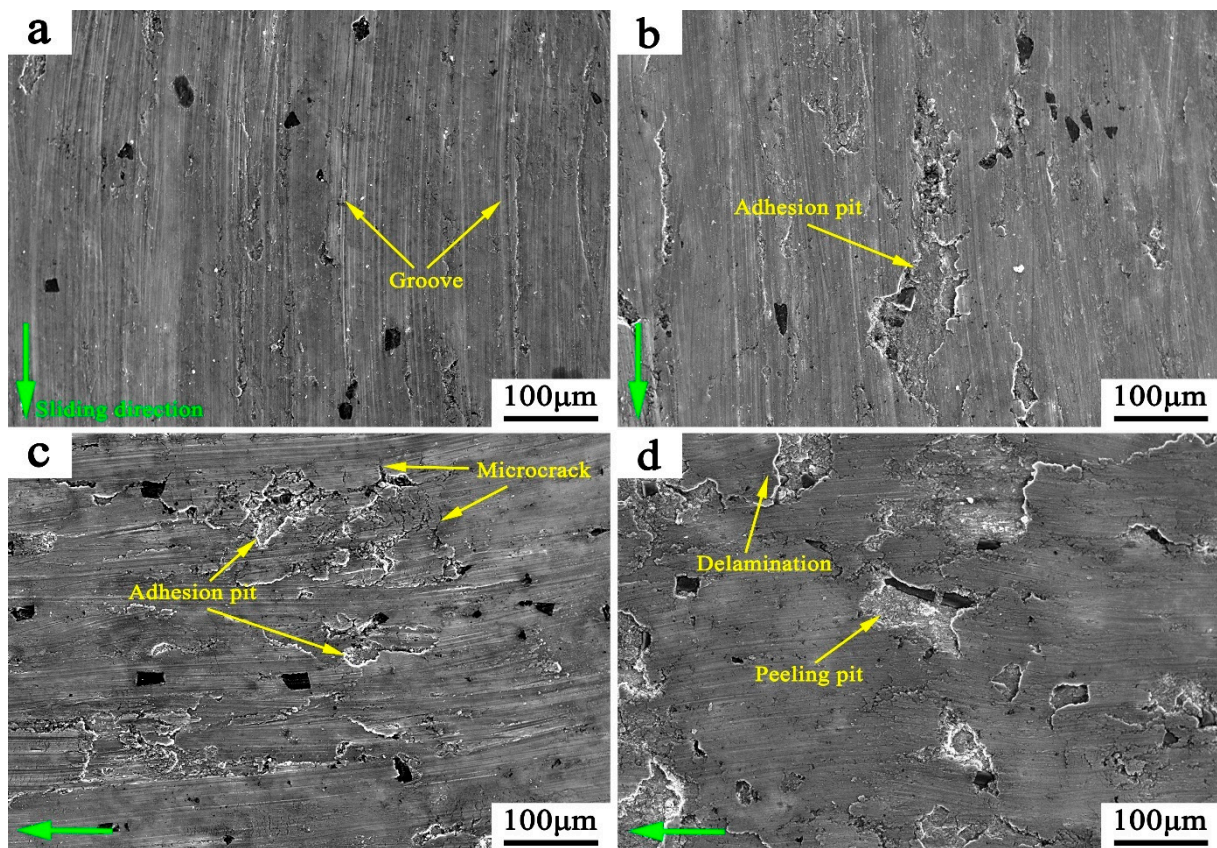


Figure 12. SEM images of the worn surface morphologies of Al-Si/CF_x composites at various rotational speeds: (a) 300 r/min; (b) 500 r/min; (c) 800 r/min; (d) 1000 r/min.

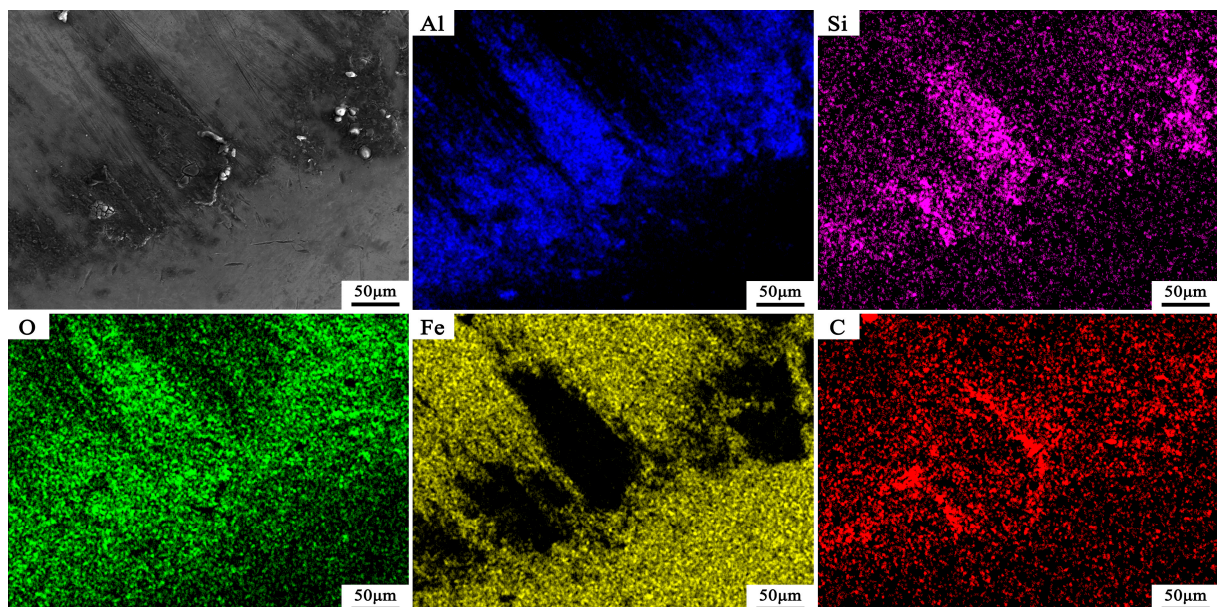


Figure 13. SEM images and EDS maps of the worn surface of the counterpart ball against the Al-Si/CF_x composite at 500 r/min.

From the above results, the tribological properties of Al-Si/CF_f composites are better than those of Al-Si/CF_p composites, but the effect of rotational speed on the wear mechanism of the two Al-Si/CF composites is roughly the same. The physical models of wear

mechanism of Al-Si/CF composites at various rotational speeds are shown in Figure 14. During the low-speed friction process, because the Al-Si/CF composite is softer than the GCr15 counterpart balls, the surface of the composite is plowed out by the asperities of the GCr15 counterpart balls to form grooves, and fine chips are generated. The chips that are transformed into abrasive grains continue to plow the surface of the material, forming a series of furrows (Figure 14a). At moderate rotational speeds, the surface temperature of the friction pair increases, and the contact point between the composite and the counterpart ball is prone to adhesion and welding. The softer composites are pulled down from the surface in the subsequent relative sliding and the adhesion pits are formed. Meanwhile, the surface layer of the composite produces plastic deformation due to undergoing a certain cyclic load, and many dislocations appear in the subsurface layer of the composite (Figure 14b). At higher rotational speed, the adhesive wear is aggravated. Moreover, the dislocation pile-up is prone to occur around the CF under the surface layer, and the initial microcracks are induced at defects such as voids and dislocation pile-up, and continuously propagates parallel to the surface under the action of shear stress parallel to the surface (Figure 14c). Under high-speed friction, the crack expands to a certain critical size or meets adjacent cracks, which will cause the material between the crack and the surface to peel off in the form of layered sheets (Figure 14d).

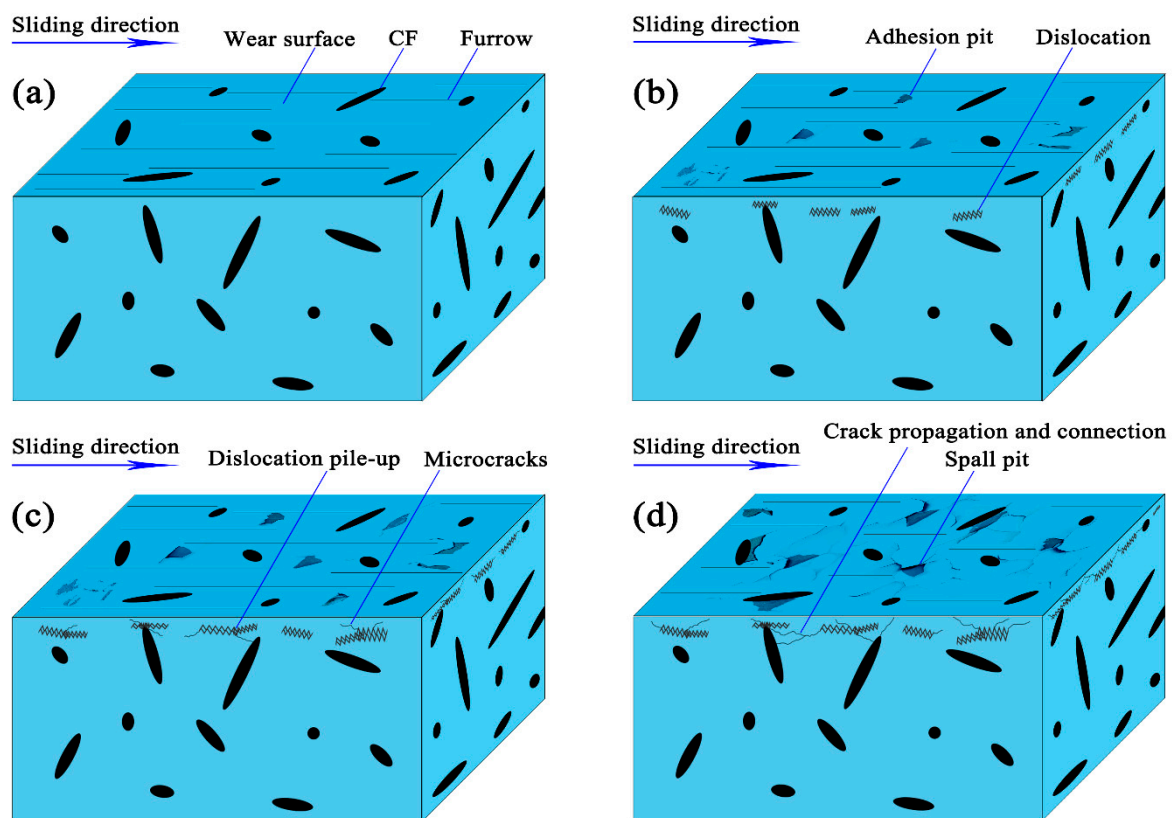


Figure 14. Physical models of wear mechanism of Al-Si/CF composites at various rotational speeds: (a) 300 r/min; (b) 500 r/min; (c) 800 r/min; (d) 1000 r/min.

Compared with the Al-Si alloy, the plastic deformation resistance of the two Al-Si/CF composites is improved and the crack nucleation is slowed down due to the pinning effect of the CF. Meanwhile, the orientation of the CFs in the composites are random. When a crack parallel to the surface encounters non-parallel CFs during propagation, the cracks will deflect along the interface between the CF and the matrix, which will hinder the propagation of microcracks and prevent more serious wear [45,48]. The CFs will be exposed when the surface material is peeled off. Hence, in the wear morphology of the two composites, we

always observed the presence of CFs at the edge of the peel pit (Figures 10d and 12d). In addition, the resistance of the CF_p to the plastic deformation of the matrix is lower than that of the CF_f due to the hollow porous structure of the CF_p. Therefore, the tribological properties of Al-Si/CF_f composites are better than those of Al-Si/CF_p composites.

4. Conclusions

The tribological properties of Al-Si/10 wt.% CF_p, Al-Si/10 wt.% CF_f composites and Al-Si alloy prepared by die casting were investigated in the rotational speed range of 300 r/min to 1000 r/min. The conclusions are as follows:

- (1) The brittle phase Al₄C₃ is not detected in the composites, which is due to the large working pressure provided by the die casting process to accelerate the wetting rate, reduce the contact time between Al melt and CFs at high temperature, and the inhibition effect of Si, Cu, Mg elements in the Al matrix. Moreover, the CFs are uniformly distributed in composites, and form a good wear-reducing and wear-resistant structure with hard-phase Si.
- (2) Compared with the Al-Si alloy, the decreases in density of the two composites and the increase in thermal conductivity are attributed to the low density and excellent thermal conductivity of the CF, and the increase in hardness is attributed to the CF restricting the grain growth and restrain the plastic flow behavior of the matrix.
- (3) With the increase in rotational speed, the COF of the Al-Si alloy and the two composites first increases and then decreases, which is attributed to the rotational speed affecting the formation of carbon film and the change in surface temperature of the friction pair. The two composites also have lower COF due to the excellent lubrication and thermal conductivity of the CF.
- (4) With the increase in rotational speed, the wear mechanisms of the Al-Si alloy and the two Al-Si/CF composites are changed from abrasive wear and adhesive wear to delamination wear. However, the CF can slow down the nucleation of cracks and prevent the propagation of microcracks, the wear mechanism changing to delamination wear of the composite requires higher rotational speeds, and the wear rate of the composite is also lower.
- (5) There is little difference in hardness and thermal conductivity of the two composites, but the density and the tribological properties of the Al-Si/CF_p composites are lower than those of the Al-Si/CF_f composites due to the hollow porous structure of the CF_p.

Author Contributions: Conceptualization, X.P. and F.T.; Methodology, G.Z. and S.X.; Validation, Y.D. and S.X.; Formal Analysis, F.T. and Z.Z.; Investigation, F.T., Y.D. and Z.Z.; Resources, Z.Z.; Data Curation, Z.Z. and Y.D.; Writing—Original Draft Preparation, F.T.; Writing—Review and Editing, X.P. and G.Z.; Visualization, F.T. and Y.D.; Supervision, X.P., G.Z. and S.X.; Project Administration, X.P.; Funding Acquisition, X.P. All authors have read and agreed to the published version of the manuscript.

Funding: This research was funded by the Provincial Technical Transformation Investment Project Foundation of Guangdong, China (Nos. 150607395130103).

Data Availability Statement: Not applicable.

Conflicts of Interest: The authors declare no conflict of interest.

References

1. Miladinović, S.; Stojanović, B.; Gajević, S.; Vencl, A. Hypereutectic Aluminum Alloys and Composites: A Review. *Silicon* **2022**. [CrossRef]
2. Zhang, M.; Tian, Y.; Zheng, X.; Zhang, Y.; Chen, L.; Wang, J. Research Progress on Multi-Component Alloying and Heat Treatment of High Strength and Toughness Al-Si-Cu-Mg Cast Aluminum Alloys. *Materials* **2023**, *16*, 1065. [CrossRef]
3. Tan, H.; Wang, S.; Yu, Y.; Cheng, J.; Zhu, S.; Qiao, Z.; Yang, J. Friction and wear properties of Al-20Si-5Fe-2Ni-Graphite solid-lubricating composite at elevated temperatures. *Tribol. Int.* **2018**, *122*, 228–235. [CrossRef]
4. Chen, X.; Zhang, Y.; Li, C.; Huang, L.; Wang, Y.; Gao, T.; Zhang, Z.; Liu, W. Wear Properties of C-MoS₂-PTFE Composite Coating Prepared on 4032 Aluminum Alloy. *Lubricants* **2022**, *10*, 181. [CrossRef]

5. Stojanovic, B.; Bukvic, M.; Epler, I. Application of Aluminum and Aluminum Alloys in Engineering. *Appl. Eng. Lett.* **2018**, *3*, 52–62. [[CrossRef](#)]
6. Wang, L.; Liu, Y.; Wu, J.; Zhang, X. Mechanical properties and friction behaviors of CNT/AlSi₁₀Mg composites produced by spark plasma sintering. *Int. J. Miner. Metall. Mater.* **2017**, *24*, 584–593. [[CrossRef](#)]
7. Shirvanimoghaddam, K.; Hamim, S.U.; Karbalaee Akbari, M.; Fakhrhoseini, S.M.; Khayyam, H.; Pakseresht, A.H.; Ghasali, E.; Zabet, M.; Munir, K.S.; Jia, S.; et al. Carbon fiber reinforced metal matrix composites: Fabrication processes and properties. *Compos. Part A Appl. Sci. Manuf.* **2017**, *92*, 70–96. [[CrossRef](#)]
8. Choi, Y.; Meng, X.; Xu, Z. Manufacturing and Performance of Carbon Short Fiber Reinforced Composite Using Various Aluminum Matrix. *J. Compos. Sci.* **2021**, *5*, 307. [[CrossRef](#)]
9. Constantin, H.; Harper, L.; Kennedy, A.R. Pressure-assisted infiltration of molten metals into non-rigid, porous carbon fibre structures. *J. Mater. Process. Technol.* **2018**, *255*, 66–75. [[CrossRef](#)]
10. Asano, K.; Zainuddin, M.F.B. Wear Behavior of PAN- and Pitch-Based Carbon Fiber Reinforced Aluminum Alloy Composites under Dry Sliding Condition. *Mater. Trans.* **2017**, *58*, 898–905. [[CrossRef](#)]
11. Manu, K.M.S.; Raag, L.A.; Rajan, T.P.D.; Pai, B.C.; Petley, V.; Verma, S.N. Self-lubricating bidirectional carbon fiber reinforced smart aluminum composites by squeeze infiltration process. *J. Mater. Sci. Technol.* **2019**, *35*, 2559–2569. [[CrossRef](#)]
12. Jang, J.M.; Ko, S.H.; Lee, W. Effects of SiC Coating of Carbon Fiber on Mechanical Properties in Short Carbon Fiber Reinforced Al Matrix Composite. *Arch. Metall. Mater.* **2021**, *66*, 941–946.
13. Zhu, C.; Su, Y.; Zhang, D.; Ouyang, Q. Effect of Al₂O₃ coating thickness on microstructural characterization and mechanical properties of continuous carbon fiber reinforced aluminum matrix composites. *Mater. Sci. Eng. A* **2020**, *793*, 139839. [[CrossRef](#)]
14. Meng, X.; Choi, Y.B.; Matsugi, K.; Xu, Z.F.; Liu, W.C. Microstructures of Carbon Fiber and Hybrid Carbon Fiber-Carbon Nanofiber Reinforced Aluminum Matrix Composites by Low Pressure Infiltration Process and Their Properties. *Mater. Trans.* **2018**, *59*, 1935–1942. [[CrossRef](#)]
15. Zhou, X.; Gao, Y.; Wang, Y.; Lu, X.; Li, Y. Fabrication and characteristic of 2024Al matrix composites reinforced by carbon fibers and ZrCp by spark plasma sintering. *J. Alloys Compd.* **2021**, *889*, 161543. [[CrossRef](#)]
16. Zhu, C.; Su, Y.; Wang, X.; Sun, H.; Ouyang, Q.; Zhang, D. Process optimization, microstructure characterization and thermal properties of mesophase pitch-based carbon fiber reinforced aluminum matrix composites fabricated by vacuum hot pressing. *Compos. B Eng.* **2021**, *215*, 108746. [[CrossRef](#)]
17. Gao, M.; Gao, P.; Wang, Y.; Lei, T.; Ouyang, C. Study on Metallurgically Prepared Copper-Coated Carbon Fibers Reinforced Aluminum Matrix Composites. *Met. Mater. Int.* **2021**, *27*, 5425–5435. [[CrossRef](#)]
18. Kumar, A.; Rana, R.S.; Purohit, R.; Saxena, K.; Xu, J.; Malik, V. Metallographic Study and Sliding Wear Optimization of Nano Si₃N₄ Reinforced High-Strength Al Metal Matrix Composites. *Lubricants* **2022**, *10*, 202. [[CrossRef](#)]
19. Li, G.; Qu, Y.; Yang, Y.; Zhou, Q.; Liu, X.; Li, R. Improved multi-orientation dispersion of short carbon fibers in aluminum matrix composites prepared with square crucible by mechanical stirring. *J. Mater. Sci. Technol.* **2020**, *40*, 81–87. [[CrossRef](#)]
20. Sree Manu, K.M.; Ajay Raag, L.; Rajan, T.P.D.; Gupta, M.; Pai, B.C. Liquid Metal Infiltration Processing of Metallic Composites: A Critical Review. *Metall. Mater. Trans. B* **2016**, *47*, 2799–2819. [[CrossRef](#)]
21. Sha, J.; Lü, Z.; Sha, R.; Zu, Y.; Dai, J.; Xian, Y.; Zhang, W.; Cui, D.; Yan, C. Improved wettability and mechanical properties of metal coated carbon fiber-reinforced aluminum matrix composites by squeeze melt infiltration technique. *Trans. Nonferr. Metal. Soc.* **2021**, *31*, 317–330. [[CrossRef](#)]
22. Galyshev, S.; Gomzin, A.; Musin, F. Aluminum Matrix Composite Reinforced by Carbon Fibers. *Mater. Today Proc.* **2019**, *11*, 281–285. [[CrossRef](#)]
23. Alten, A.; Erzi, E.; Gürsoy, Ö.; Hapçı Ağaoğlu, G.; Dispinar, D.; Orhan, G. Production and mechanical characterization of Ni-coated carbon fibers reinforced Al-6063 alloy matrix composites. *J. Alloys Compd.* **2019**, *787*, 543–550. [[CrossRef](#)]
24. Patil, N.A.; Pedapati, S.R.; Marode, R.V. Wear Analysis of Friction Stir Processed AA7075-SiC-Graphite Hybrid Surface Composites. *Lubricants* **2022**, *10*, 267. [[CrossRef](#)]
25. Yang, Q.; Liu, J.; Li, S.; Wang, F.; Wu, T. Fabrication and mechanical properties of Cu-coated woven carbon fibers reinforced aluminum alloy composite. *Mater. Des.* **2014**, *57*, 442–448. [[CrossRef](#)]
26. Zhong, K.; Zhou, J.; Zhao, C.; Yun, K.; Qi, L. The effect of nickel coating on the mechanical properties and failure modes of continuous carbon fiber reinforced aluminum matrix composites. *J. Alloys Compd.* **2022**, *904*, 164134. [[CrossRef](#)]
27. Bedmar, J.; Torres, B.; Rams, J. Manufacturing of Aluminum Matrix Composites Reinforced with Carbon Fiber Fabrics by High Pressure Die Casting. *Materials* **2022**, *15*, 3400. [[CrossRef](#)]
28. Eid, M.; Kaytbay, S.; Elkady, O.; El-Assal, A. Microstructure and mechanical properties of CF/Al composites fabricated by hot coining technique. *Ceram. Int.* **2021**, *47*, 21890–21904. [[CrossRef](#)]
29. Deng, Y.; Pan, X.; Zeng, G.; Liu, J.; Xiao, S.; Zhou, Z. Study on high-temperature wear and mechanism of Al-Si/graphite composites prepared by the die-casting process. *Ind. Lubr. Tribol.* **2020**, *72*, 1153–1158. [[CrossRef](#)]
30. Liu, Y.; Du, J.; Yu, S.; Wang, W. High temperature friction and wear behaviour of Al₂O₃ and/or carbon short fibre reinforced Al-12Si alloy composites. *Wear* **2004**, *256*, 275–285.
31. Du, J.; Liu, Y.; Yu, S.; Li, W. Dry sliding friction and wear properties of Al₂O₃ and carbon short fibres reinforced Al-12Si alloy hybrid composites. *Wear* **2004**, *257*, 930–940.

32. Samal, P.; Vundavilli, P.R.; Meher, A.; Mahapatra, M.M. Recent progress in aluminum metal matrix composites: A review on processing, mechanical and wear properties. *J. Manuf. Process.* **2020**, *59*, 131–152. [[CrossRef](#)]
33. Stojanović, B.; Ivanović, L. Application of aluminium hybrid composites in automotive industry. *Teh. Vjesn.* **2015**, *22*, 247–251. [[CrossRef](#)]
34. Wei, W.; Liao, Q.; Yang, Z.; Li, X.; Huang, Z.; Ren, J.; Yang, Y.; Wu, G. Interfacial modification and performance enhancement of carbon matrix/aluminum composites. *J. Alloys Compd.* **2022**, *903*, 163877. [[CrossRef](#)]
35. Chen, S.; An, Q.; Shen, P. Influences of Si and Ti on the wettability and reactivity of Al/graphite system at 900 °C. *Materialia* **2021**, *16*, 101060. [[CrossRef](#)]
36. Yu, Z.; Tan, Z.; Xu, R.; Ji, G.; Fan, G.; Xiong, D.; Guo, Q.; Li, Z.; Zhang, D. Enhanced load transfer by designing mechanical interfacial bonding in carbon nanotube reinforced aluminum composites. *Carbon* **2019**, *146*, 155–161. [[CrossRef](#)]
37. Kaczmar, J.W.; Naplocha, K.; Morgiel, J. Microstructure and Strength of Al₂O₃ and Carbon Fiber Reinforced 2024 Aluminum Alloy Composites. *J. Mater. Eng. Perform.* **2014**, *23*, 2801–2808. [[CrossRef](#)]
38. Wang, C.; Chen, G.; Wang, X.; Zhang, Y.; Yang, W.; Wu, G. Effect of Mg Content on the Thermodynamics of Interface Reaction in Cf/Al Composite. *Metall. Mater. Trans. A Phys. Metall. Mater. Sci.* **2012**, *43*, 2514–2519. [[CrossRef](#)]
39. Eid, M.; Kaytbay, S.; El-Assal, A.; Elkady, O. Electrical, Thermal, and Mechanical Characterization of Hot Coined Carbon Fiber Reinforced Pure Aluminium Composites. *Met. Mater. Int.* **2022**, *28*, 2747–2765. [[CrossRef](#)]
40. Miranda, A.T.; Bolzoni, L.; Barekar, N.; Huang, Y.; Shin, J.; Ko, S.; McKay, B.J. Processing, structure and thermal conductivity correlation in carbon fibre reinforced aluminium metal matrix composites. *Mater. Des.* **2018**, *156*, 329–339. [[CrossRef](#)]
41. Lee, M.; Choi, Y.; Sugio, K.; Sugio, K.; Matsugi, K.; Sasaki, G. Effect of aluminum carbide on thermal conductivity of the unidirectional CF/Al composites fabricated by low pressure infiltration process. *Compos. Sci. Technol.* **2014**, *97*, 1–5. [[CrossRef](#)]
42. Xie, W.; Cheng, H.F.; Chu, Z.Y.; Chen, Z.H.; Zhou, Y.J.; Long, C.G. Comparison of Hollow-Porous and Solid Carbon Fibers as Microwave Absorbents. *Adv. Mat. Res.* **2010**, *150*, 1336–1342. [[CrossRef](#)]
43. Zeng, X.; Yu, J.; Fu, D.; Zhang, H.; Teng, J. Wear characteristics of hybrid aluminum-matrix composites reinforced with well-dispersed reduced graphene oxide nanosheets and silicon carbide particulates. *Vacuum* **2018**, *155*, 364–375. [[CrossRef](#)]
44. Schön, J. Coefficient of friction for aluminum in contact with a carbon fiber epoxy composite. *Tribol. Int.* **2004**, *37*, 395–404. [[CrossRef](#)]
45. Cao, X.; Shi, Q.; Liu, D.; Feng, Z.; Liu, Q.; Chen, G. Fabrication of in situ carbon fiber/aluminum composites via friction stir processing: Evaluation of microstructural, mechanical and tribological behaviors. *Compos. B Eng.* **2018**, *139*, 97–105. [[CrossRef](#)]
46. Akbarzadeh, E.; Picas, J.A.; Baile, M.T. Orthogonal experimental design applied for wear characterization of aluminum/C_{sf} metal composite fabricated by the thixomixing method. *Int. J. Mater. Form.* **2016**, *9*, 601–612. [[CrossRef](#)]
47. Ramesh, C.S.; Adarsha, H.; Pramod, S.; Khan, Z. Tribological characteristics of innovative Al6061–carbon fiber rod metal matrix composites. *Mater. Des.* **2013**, *50*, 597–605. [[CrossRef](#)]
48. Zhang, Z.; Wang, Q.; Dong, S.; Yu, Z.; Zhang, Q.; Zhang, P.; Wang, X.; Zhang, B.; Li, X.; Liang, Y.; et al. The effect of carbon fiber strengthening on the mechanical properties and wear resistance of 24CrNiMo alloy steel fabricated by laser deposition. *J. Mater. Res. Technol.* **2020**, *9*, 9117–9128. [[CrossRef](#)]

Disclaimer/Publisher’s Note: The statements, opinions and data contained in all publications are solely those of the individual author(s) and contributor(s) and not of MDPI and/or the editor(s). MDPI and/or the editor(s) disclaim responsibility for any injury to people or property resulting from any ideas, methods, instructions or products referred to in the content.